Xueshan Gao
Mingda Miao ✉
Peng Zhao
Pengfei Zhang

https://doi.org/10.21278/TOF.481042022
ISSN 1333-1124
eISSN 1849-1391

OPTIMIZATION ANALYSIS OF THE STRUCTURAL DESIGN AND STABILITY PARAMETERS OF A REHABILITATION ROBOT

Summary

In this paper, a lower limb rehabilitation robot, suitable for stroke patients, is designed to meet the needs of the lower limb training in a later stage of rehabilitation. The rehabilitation robot is composed of a gantry structure, a driving system, a weight support system, and a human-computer interaction system. Such a robot can assist the patients to stand and walk on the ground. Because of the weakness of the lower limbs on the affected side, stroke patients find it difficult to maintain their own body balance. The patients may fall due to a change in body posture caused by insufficient body function. Therefore, it is necessary to evaluate the stability of the rehabilitation robot after being impacted by the patient's fall during use. This paper presents a method for the analysis of robot stability and develops an approximate mathematical model of the rehabilitation robot stability based on the response surface method. Optimal structural design parameters for the rehabilitation robot under impact are determined based on the response surface mathematical model. Finally, a stability experiment of the rehabilitation robot under the optimal structural parameters is performed. The experimental results demonstrate that the universal wheel maintains a close force contact with the ground, which proves the reliable stability of the robot.

Key words: *rehabilitation robots, structural design, response surface method, stability parameters, optimization analysis*

1. Introduction

The incidence of stroke, a common neurological disease, is high and so are the stroke mortality and disability rates. With the development of medical technology, the survival rate of stroke patients has gradually increased. However, almost 90% of stroke survivors suffer from some motor impairment, which not only affects their daily life but also increases the risk of falls [1]. Consequently, early intervention and rehabilitation treatment can efficiently reduce the chances of becoming disabled. With a gradual increase in the number of people with motor impairment, the rehabilitation treatment of stroke patients becomes more important [2]. The traditional rehabilitation treatment is mostly performed manually or using simple medical equipment. This method is time-consuming and physical therapists are costly [3, 4]. In addition, it mainly relies on manual assistance. Therefore, the experience of physiotherapists determines the rehabilitation effect. Due

to a lack of objective data for scientific evaluation of the training parameters and rehabilitation effect, it is difficult to optimize the training scheme in order to obtain the highest treatment performance [5]. This limits the accuracy and efficiency of the rehabilitation training.

In recent years, robots have been widely used in the field of rehabilitation. Several researchers used modern biomedical engineering and robot technology for stroke rehabilitation [6]. The rehabilitation robot can meet the needs of efficient, targeted, and continuous rehabilitation training. It can also improve the rehabilitation efficiency, reduce the rehabilitation cost, and perform several active and passive training modes. Compared with the traditional rehabilitation treatment, the rehabilitation robot can maintain the consistency of the rehabilitation training and independently complete the cumbersome and time-intensive treatment of patients. The robot-assisted rehabilitation is a better training method [7]. The authors of [8] proposed a robot mobile platform which could provide social assistance and accompany its users. This mobile platform had a weight support device, which could move according to the user's motion information, monitor the user's training progress, adapt to the user's walking in a similar way to the therapist, and improve the user's comfort and independence in training. An exoskeleton mobile robot platform for an upper limb robot, which used a modular design to meet the needs of each user, was proposed in [9]. Based on the virtual home environment to simulate the user interaction with household items, the platform system was too complex and cumbersome, and therefore it should be improved and optimized. The authors of [10] proposed a walking assistant robot with a walking stick to follow the user, which could assist and supervise patients with lower limb dysfunction to walk long distance by estimating the human walking intention. However, this robot was only suitable for patients who recovered to the stage of independent walking and could not provide patients with body weight support and more reliable safety protection. The authors of [11] proposed a mobile ground gait training system. They tested the feasibility and control stability of the developed system based on the prototype model. The designed system included a mobile electric walker, a weight support system and an exoskeleton gait orthosis, which could perform several ground gait training functions. The experiments demonstrated that the robot could provide weight support according to the user's gait training needs and help the user to perform ground gait training. For the recognition of human motion, it is very important to design an intelligent wearable device that can provide recognition help [12, 13]. At the same time, through the body's sensor network, this device could also monitor the user's state in real time or identify the walking activities [14] and gait events performed by the user [15]. This method became an indispensable part of intelligent medical services [16]. The prototypes and products of the recent lower limb rehabilitation robots are summarized in [17]. The advantages and disadvantages of the theories and technologies used in these studies were compared. In addition, the functional characteristics of the equipment and the aspects that should be improved were analysed. The authors of [18-21] considered the structural size and parametric connecting components of the robot as influencing factors. In addition, they optimized the structural parameters of the robot by constructing a multi-objective optimization function, which improved the global performance of the robot. In traditional industries, the process of designing, verifying, and manufacturing a product can be lengthy and expensive, and some common approaches to solving these problems are parametric product modelling and finite element analysis [22]. The author of [23] used the response surface methodology to determine a mathematical model for multi-objective pollutants, researched the air quality inside passenger cars, obtained the relationship between the air quality inside the car and pollutants, and proposed solutions to improve the air quality inside the car. To reduce the influence of human factors in multi-objective optimization problems, the author [24] proposed a non-dominant sorting genetic algorithm, the analytic hierarchy process method. By establishing a multi-objective optimization model for the optimization object, the goal of selecting Pareto solution sets was achieved, effectively solving multi-objective problems in the structural optimization design. It can be seen from the above literature that stroke patients need targeted, repeated, and intensive active training to strengthen

the neural pathway of the brain, in order to achieve the reconstruction of the limb motor function. However, the long-term care provided by relatives or professionals is very costly for the patients.

In order to really understand and get familiar with the needs and problems in the field of rehabilitation, in the early stage of the study, we spent some time conducting research in the hospital rehabilitation department, during which we had in-depth communication with many stroke patients, their families and rehabilitation physicians. We learned that stroke patients need to take active walking rehabilitation training under the guidance of doctors at the late stage of rehabilitation training. In the process of rehabilitation, a patient needs to be accompanied and guided by multiple rehabilitation physicians to ensure the patient's safety and rehabilitation effect. Due to a small number of rehabilitation physicians, there are many patients who have to wait for their rehabilitation training or even cannot get any rehabilitation training guidance. To address the rehabilitation needs of stroke patients in the later period of the rehabilitation training, reduce the workload of rehabilitation physicians and improve the efficiency of the rehabilitation treatment, it is necessary to develop a lower limb rehabilitation training robot with high motor flexibility, robust structural stability and the ability to provide weight support for patients. The existing lower extremity rehabilitation robots mainly focus on passive rehabilitation training and fixed suspension rehabilitation training. Patients are under the restraint of rope suspension combined with a treadmill to carry out passive forms of fixed rehabilitation training, and thus the boring environment makes it impossible for them to obtain a good training mentality and rehabilitation results. The common active rehabilitation training equipment has a simple rehabilitation form and a single application object because of which it is difficult to meet the needs of stroke patients with complex conditions at different stages. The proposed mobile lower limb rehabilitation robot can sense the patients' rehabilitation intentions, integrate patients' independent rehabilitation ideas into the training, enhance the patients' active enthusiasm in the rehabilitation treatment process, and provide personalized training methods. The patients can perform active lower limb motion rehabilitation while relying on the rehabilitation robot to achieve their own weight loss and balance. They can also control the robot to move in its desired direction to perform the exercise mode of free walking on the ground.

Compared with fixed treadmill-based rehabilitation robots, mobile robots have the possibility of overturning when impacted by a patient's fall. The safety and reliability of the rehabilitation equipment are extremely important in the field of rehabilitation. Therefore, we need to pay special attention to and improve the safety and reliability of rehabilitation robots when they are impacted by external forces. However, we cannot blindly pursue safety and reliability, which would result in a redundant design. The redundant design will make the rehabilitation equipment very cumbersome, thus affecting the flexibility and the effect of using the equipment. Therefore, it is necessary to explore the optimal parameters for the safety design of the rehabilitation robot. To reduce the design redundancy and improve the design efficiency of the rehabilitation robot, the structural stability and design parameters of the rehabilitation robot need to be optimized. In this paper, the response surface method is used to construct a stability optimization approximate model while using the force value of the robot driving wheel as the objective function, and the mass of the robot, the weight of stroke patients, the elastic coefficient of the body weight support system (BWSS), and the force of the universal wheel as the constraint functions. Optimal structural design parameters for the rehabilitation robot under impact were determined based on the response surface mathematical model. Finally, the stability experiment of the rehabilitation robot under the optimal structural parameters is performed.

The remainder of this paper is organized as follows. In Section 2, a design framework of the rehabilitation robot system that is suitable for patients with lower limb dysfunction is proposed. In addition, the mechanical design of the rehabilitation robot is introduced. In Section 3, three parameter variables affecting the stability of the rehabilitation robot are proposed: the robot mass, the patient weight and the elastic coefficient of the weight support system. Based on the response surface method, the second-order response surface mathematical

model of the rehabilitation robot stability with respect to the influencing parameters is established. In Section 4, the robot flexibility and stability are verified by experiments, based on the rehabilitation robot prototype. Finally, the conclusion is drawn in Section 5.

2. Rehabilitation robotic system design

2.1 Design requirements and factors

In general, stroke patients have unilateral motor dysfunction. During the rehabilitation training, they often fall due to the imbalance of the centre of gravity, caused by the instability of one limb of the body. The lack of the self-protection ability of patients can easily cause injuries. Therefore, the safety of patients is very important, which also puts forward strict requirements for the safety of the rehabilitation robots. The safety of patients should be considered in each stage of the robot design. For some patients who are unable to stand and walk due to insufficient strength of lower limbs, physiotherapists can use rehabilitation robots to apply auxiliary assistance depending on their condition. Consequently, the balance of the body is ensured and the standing state is performed while the burden of the lower limbs during walking is reduced. In addition, the rehabilitation environments of the rehabilitation robot and the patients are mostly indoors, which requires a high flexibility of the rehabilitation robot. Moreover, when the patient accidentally falls due to insufficient strength of the lower limbs, the protection mechanism of the robot can protect the patient from injuries. Therefore, the robot should be designed as an independent platform with a compact structure and sufficient safety, stability, and flexible movement, so as to be efficiently used in flat indoor and outdoor fields. Finally, the robot should also meet the requirements of patients using wheelchairs [25].

To meet the trafficability of the robot in its environment and the application needs of patients using wheelchairs, the size of the rehabilitation robot is determined according to the reference data extracted from [26, 27]. The paper considers the average body shape standards of people in Asia and Europe as well as the elevator standards, so as to ensure that the robot can efficiently move between rooms, elevators and buildings in the public environment. In the case of inaccessible areas, the robot can be disassembled and re-assembled. To ensure that the robot meets the requirements of the rehabilitation function, its design should first consider the safety problem, followed by the mechanism optimization problem. Furthermore, patients of different races, heights and ages can use this robot. In other words, its structural design can adapt to different users. Finally, it can provide personalized rehabilitation treatment for stroke patients, so that the lower limb motor function of the patients can gradually recover and adapt to the walking state.

2.2 Robot structural design

The rehabilitation robot is composed of a gantry body structure, a driving system, a BWSS and a human-computer interaction system (HCIS). The structural design of the mobile platform is illustrated in Figure 1. The robot uses the gantry structure design, with an overall external size of 120 × 98 × 180 cm and an internal size of 76 cm, which can help the patient to use the wheelchair. In order to reduce the centre of gravity of the robot and improve the stability of the equipment, the upper structure of the gantry is made of an aluminium profile while the base is made of steel. Two driving wheels are installed in the middle of the robot base, and four non-central universal wheels are installed at the front and rear to jointly carry the self-weight and load of the robot. The driving system uses the central driving form, which allows the robot to perform the small radius or in-situ steering and highly improves its mobile flexibility. The weight support system uses an independent symmetrical design, according to the patient's unilateral rehabilitation needs on the left or the right side of the body. The system is composed of a servo motor, a worm gear reducer, a force sensor, a steel wire rope, a displacement sensor, a fixed shaft pulley, a pulley moving pair, a tension spring, a linear guide rail and a traction arm. The worm gear reducer is installed between the servo motor and the winding wheel to ensure that the system has a sufficient output torque. The traction arm is equipped with a linear

guide rail module and a displacement sensor. The displacement sensor is installed at the end of the linear guide rail of the traction arm. The weight reducing clothing is connected to the moving pair on the linear guide rail. When the human body moves, it drives the moving pair to slide. The displacement sensor generates displacement changes, identifies the motion state of the patient accordingly, and controls the robot motion [25]. The robot weight support and the HCI system are presented in Figure 2. The use of the rehabilitation robot is illustrated in Figure 3.

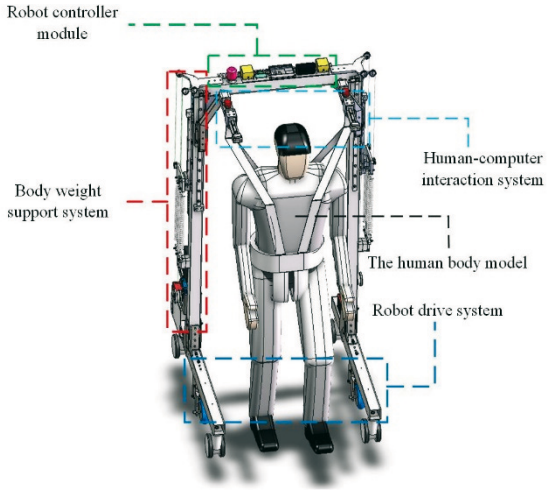

Fig. 1 Rehabilitation robot platform system

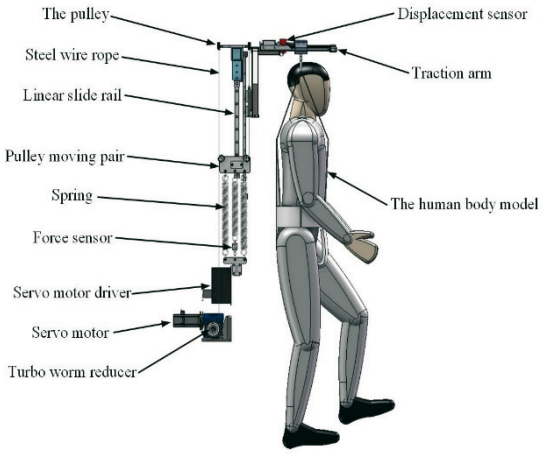

Fig. 2 BWSS and HCIS of the rehabilitation robot

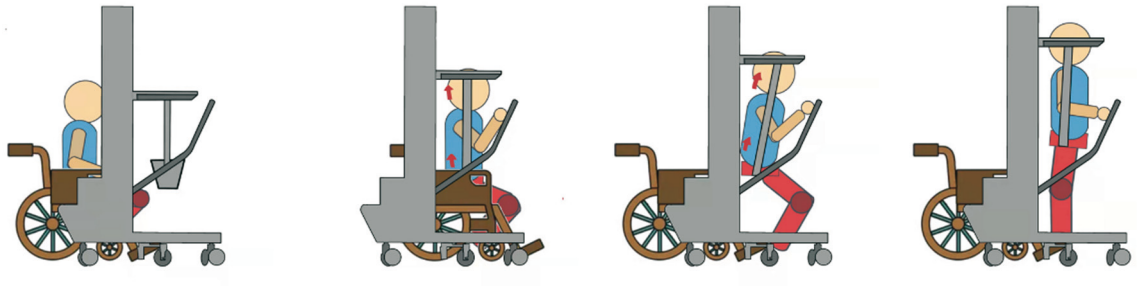

Fig. 3 Application method of the rehabilitation robot

The research topic of this paper is a mobile rehabilitation robot with a six-wheel structure. Four universal wheels (O_1, O_2, O_3, and O_4) are located in the front and rear positions of the robot, while two driving wheels (O_5 and O_6) are located in its middle position. The dimensions of the rehabilitation robot structure are simplified, as shown in Figure 4.

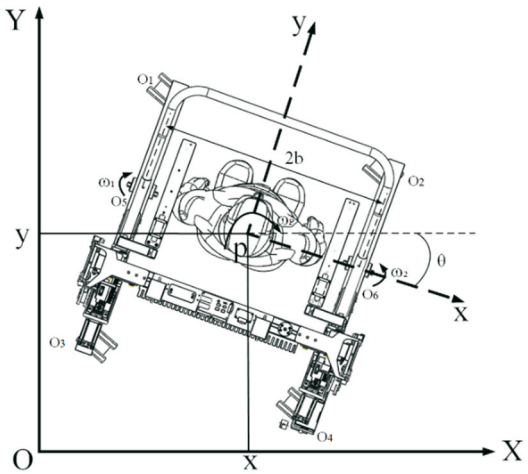

Fig. 4 Schematic diagram of dimensions of the robot structure

3. Stability parameter analysis of the rehabilitation robot

Because of the widespread unilateral motor dysfunction, stroke patients often fall during the walking rehabilitation training due to the imbalance of the centre of gravity caused by the instability of the affected lower limb. The patients can then be easily injured because their self-protection ability is insufficient. Based on the potential hidden safety hazards, it is necessary to assess the structural stability of the rehabilitation robot when affected by the patient's fall.

3.1 Variables and scoping

In the design of the robot, the overall size of the robot remains unchanged and the positions of all parts are fixed. In general, the greater the mass of the robot base and the lower the robot centre of gravity, the greater the stability. In addition, when the patient's height remains unchanged, the greater the weight, the higher the impact on the robot when falling, which in turn has a high impact on the stability of the robot mechanism. Moreover, the elastic coefficient in the weight balance support system affects the acceleration when the patient falls. The smaller the elastic coefficient, the greater the acceleration when the patient falls, which is also an important factor leading to the robot instability. Therefore, this paper studies the impact on the stability of the robot under the action of these three factors. The main factors affecting the stability of the robot are the quality of the robot, the weight of the patient and the elastic coefficient of the weight support system.

For the purpose of easy transportation of rehabilitation robots, their structural mass range is set to 100-150 kg, while the user's weight range is set to 50 ~ 100 kg, based on the average body shape standard parameters of the Asian and European populations [26, 27]. To ensure that the rehabilitation robot provides appropriate weight support to patients, the adjustment range of the weight balance support system is set to 0 ~ 60 kg and the maximum spring shape variable of the weight support system is set to 300 mm. According to Hooke's law, the minimum elastic coefficient of the rehabilitation robot is almost 2 N/mm and the safety factor is 1.2 while the requirements of the maximum weight support are met. When the weight balance support system supports the weight of 100 kg patients, the elastic coefficient is 4 N/mm. The mass of the robot, the weight of the patient, and the elastic coefficient of the BWSS are determined as the parameter variables affecting the robot stability. The optimal value range of each target test factor is $x_1 \in [100,150]$, $x_2 \in [50,100]$ and $x_3 \in [2, 4]$. The design test factors and levels are presented in Table 1.

Table 1 Design test factors and levels

Variable	x_1 Robot mass/kg	x_2 Patient weight/kg	x_3 Coefficient of elasticity N/mm
maximum values	150	100	4
minimum values	100	50	2

The response surface analysis determines the explicit polynomial equation of an implicit function, by screening the iteration and the test points. It is necessary to analyse the stability of the rehabilitation robot to obtain corresponding optimal parameters. First, the maximum contact force (M) acting between the driving wheel of the rehabilitation robot and the ground is considered as the objective function. Since the stability of the rehabilitation robot is related to its quality, the weight of the patient, and the elastic coefficient of the weight support system, the contact force acting between the universal wheel of the rehabilitation robot and the ground is limited to the allowable range. That is, the contact force is greater than 0 N. When the contact force is zero, it can be considered that the wheel is separated from the ground, and therefore it does not meet the stability requirements. In addition, to ensure the friction between the robot driving wheel and the ground and prevent the driving wheel from slipping, the contact force acting between the driving wheel and the ground should be greater than 150 N. Based on the

above analysis of the stability characteristics of the rehabilitation robot, the mathematical relationship between the robot mass, the patient's weight, and the elastic coefficient of the weight support system and the robot driving wheel, the universal wheel and the ground contact force is studied, and a mathematical model of the stability of the rehabilitation robot is established as follows:

$$\begin{aligned} &\max M(x_1, x_2, x_3) \\ &s.\ t \begin{cases} Y_1(x_1, x_2, x_3) \geq f_{\min} \\ Y_2(x_1, x_2, x_3) \geq f_{\min} \\ Y_3(x_1, x_2, x_3) \geq f_{\min} \\ Y_4(x_1, x_2, x_3) \geq f_{\min} \\ 100\ \text{kg} \leq x_1 \leq 150\ \text{kg} \\ 50\ \text{kg} \leq x_2 \leq 100\ \text{kg} \\ 2\ \text{N/mm} \leq x_3 \leq 4\ \text{N/mm} \end{cases} \end{aligned} \tag{1}$$

where x_1, x_2, and x_3 are the robot mass, the patient's weight, and the elasticity coefficient, respectively; $f_{\min}$ is the minimum contact force acting between the universal wheel and the ground; M is the objective function of the maximum contact force acting between the robot driving wheel and the ground, which is the average of the maximum contact force M_1 acting between the robot driving wheel O_5 and the ground and the maximum contact force M_2 acting between O_6 and the ground; Y_1, Y_2, Y_3, and Y_4 are the constraint functions of the contact force acting between the robot universal wheels O_1, O_2, O_3, and O_4 and the ground, respectively.

3.2 Box-Behnken design test and arrangement

This section studies the influence of the free fall of subjects having the same height (180 cm) and different weights on the force acting between the robot wheel and the ground. The change in the contact force acting between the robot universal wheels O_1, O_2, O_3, and O_4 and the ground is measured. The minimum value of the contact force is recorded. The change in the indirect contact force acting between the robot driving wheel and the ground is also measured, and the maximum value of the contact force is recorded. The response surface design method is usually used to improve the model after the important factors are determined by using screening design or factor design. There are two main types of response surface design, namely, the central composite design and the Box-Behnken design (BBD). The BBD has a processing combination located at the midpoint of the edge of the test space and it requires at least three continuous factors. Therefore, the BBD test method is adopted in this paper and the test schedule is shown in Table 2. Note that 17 tests are required. The initial condition of the test is that the subjects are in the balanced state of the weight support and the weight reduction is set to 300 N.

Table 2 Test and results of BBD

No	x_1/kg	x_2/kg	x_3/N/mm	Y_1/N	Y_2/N	Y_3/N	Y_4/N	M
1	125.00	100.00	4.00	384.80	312.84	245.24	177.79	159.44
2	125.00	50.00	2.00	291.79	236.75	223.34	161.64	158.30
3	125.00	75.00	3.00	325.58	267.47	230.03	170.55	160.62
4	150.00	75.00	2.00	318.49	250.26	260.00	161.19	157.90
5	100.00	100.00	3.00	283.33	237.72	193.12	155.26	160.90
6	125.00	75.00	3.00	325.58	267.47	230.03	170.55	160.78
7	150.00	100.0	3.00	380.20	278.17	274.65	169.00	157.57
8	150.00	50.00	3.00	363.78	280.56	272.80	178.80	157.96
9	125.00	75.00	3.00	325.50	267.47	230.03	170.55	161.09

No	x_1/kg	x_2/kg	x_3/N/mm	Y_1/N	Y_2/N	Y_3/N	Y_4/N	M
10	125.00	75.00	3.00	325.58	267.47	230.03	170.50	160.97
11	100.00	75.00	4.00	325.69	277.96	200.19	174.80	161.71
12	150.00	75.00	4.00	424.64	339.69	287.90	186.74	158.81
13	125.00	100.00	2.00	273.59	221.94	220.53	147.11	159.45
14	100.00	50.00	3.00	271.75	233.98	190.33	160.66	160.55
15	100.00	75.00	2.00	233.34	196.96	188.24	143.05	160.90
16	125.00	50.00	4.00	355.73	303.62	238.50	185.89	160.37
17	125.00	75.00	3.00	325.58	267.47	230.03	170.55	160.74

3.3 Development of the response surface model

According to the results of the robot stability analysis obtained from the experimental design and the arrangement in Table 2, the response surface equation is developed by using the analysis software. In addition, a response surface model (RSM) of the constraint functions (Y_1, Y_2, Y_3, and Y_4) of the contact force acting between the rehabilitation robot wheel and the ground as well as the objective function (M) of the maximum contact force acting between the rehabilitation robot driving wheel and the ground is developed. The results are given by the following equations:

$$M(x_1,x_2,x_3)=132.17+0.19x_1+0.34x_2+4.5x_3-2.96\times10^{-4}x_1x_2 \\ +1\times10^{-3}x_1x_3-0.02x_2x_3-9.24\times10^{-4}x_1^2-1.63\times10^{-3}x_2^2-0.43x_3^2 \tag{2}$$

$$Y_1(x_1,x_2,x_3)=100.52+1.65x_1-1.48x_2-11.06x_3+1.93\times10^{-3}x_1x_2 \\ +0.14x_1x_3+0.47x_2x_3-1.39\times10^{-3}x_1^2+1.11\times10^{-4}x_2^2+0.84x_3^2 \tag{3}$$

$$Y_2(x_1,x_2,x_3)=-61.16+3.43x_1+0.44x_2-17.32x_3-2.45\times10^{-3}x_1x_2 \\ +0.08x_1x_3+0.24x_2x_3-9.95\times10^{-3}x_1^2-5.83\times10^{-3}x_2^2+4.96x_3^2 \tag{4}$$

$$Y_3(x_1,x_2,x_3)=150.32+0.19x_1-0.26x_2-26.82x_3-3.76\times10^{-4}x_1x_2 \\ +0.16x_1x_3+0.10x_2x_3+3.90\times10^{-3}x_1^2+4.12\times10^{-3}x_2^2+1.62x_3^2 \tag{5}$$

$$Y_4(x_1,x_2,x_3)=-21.67+1.88x_1+0.19x_2+22.71x_3-1.76\times10^{-3}x_1x_2 \\ -0.06x_1x_3+0.06x_2x_3-5.02\times10^{-3}x_1^2-2.36\times10^{-3}x_2^2-0.96x_3^2 \tag{6}$$

where M, Y_1, Y_2, Y_3, and Y_4 represent the contact force acting between the driving wheel, wheel O_1, wheel O_2, wheel O_3, wheel O_4, and the ground, respectively, and x_1, x_2, and x_3 are the mass of the robot, the weight of the patient and the stiffness coefficient of the spring, respectively.

To verify that the established RSM of the maximum contact force acting between the robot driving wheel and the ground can truly reflect the statistical law between the response surface and the design factors, a variance analysis of Equation (2) is performed and the significance of the linear, square, and cross terms is analysed. The RSM of the objective function m is analysed by variance. The obtained results are presented in Table 3.

Table 3 Results of *M* analysis of variance

Source	Sum of squares	Mean square	*F* value	*P* value
model	27.67	3.07	130.93	< 0.0001
x_1	17.46	17.46	743.83	< 0.0001
x_2	0.004	0.004	0.17	0.6903
x_3	1.79	1.79	76.07	< 0.0001
x_1x_2	0.14	0.14	5.83	0.0465
x_1x_3	0.0025	0.00025	0.11	0.7537
x_2x_3	1.08	1.08	46.07	0.0003
x_1^2	1.40	1.40	59.81	0.0001
x_2^2	4.36	4.36	185.67	< 0.0001
x_3^2	0.79	0.79	33.55	0.0007
Lack of fit	0.023	0.0076	0.22	0.8805

For the RSM of the maximum contact force acting between the robot driving wheel and the ground, it can be seen from Table 3 that the *F* value of the RSM is 130.93 and the *P* value is less than 0.0001. This indicates that the model highly affects the maximum contact force acting between the driving wheel and the ground and it has a high reliability. In addition, the *P* values of the robot mass x_1 and elastic coefficient x_3 are less than 0.0001. This indicates that these two factors highly affect the RSM (*M)*. The *P* value of the model misalignment term is 0.8805, which indicates that the misalignment of the model is not significant, and therefore the response surface approximation model *M* has an accurate fitting effect on the maximum contact force acting between the driving wheel and the ground. Consequently, the test error is relatively small.

In the statistical analysis of the regression equation error, *Std. Dev.* represents the standard variance, *Mean* denotes the average value, C.V% is the coefficient of variation, *PRESS* represents the sum of squares of errors, and R^2 denotes the correlation coefficient which is used to evaluate the fitting effect of the mathematical model. An R^2 value close to 1 indicates that the fitting effect of the RSM is better [28]. Note that *Adeq Precision* determines the model resolution. A signal-to-noise ratio greater than 4 indicates a high resolution of the RSM. In addition, high values of *Adj* R^2 and *Pred* R^2 and a difference between them which is lower than 0.2 indicate that the model interpretation is more sufficient [29]. It can be seen from Table 4 that the correlation coefficient R^2 of the response surface function of the maximum contact force acting between the robot driving wheel and the ground is 0.9941. Moreover, *Adj* R^2 is equal to 0.9865. This indicates that the RSM fits well the contact force acting between the driving wheel and the ground. The signal-to-noise ratio of the RSM is 35.093, which indicates that the RSM can be used to fit the contact force acting between the driving wheel and the ground. That is, the RSM can be used for the correlation analysis and prediction of the contact force acting between the driving wheel and the ground. The coefficient of variation is 1.56%. The response surface function can better represent the contact force acting between the driving wheel and the ground. Therefore, the reliability of the RSM is high. Furthermore, the difference between *Adj* R^2 and *Pred* R^2 in the function is 0.0076 and the deviation between them is very small. The RSM does not need to be further optimized.

It can be seen from Tables 5-8 that the correlation coefficients of the Y_1, Y_2, Y_3, and Y_4 response surface functions are 0.9970, 0.9935, 0.9998, and 0.9966, respectively, while the values of *Adj* R^2 are 0.9931, 0.9952, 0.9996, and 0.9921, respectively. This indicates that the RSM has accurate fitting results for the maximum contact force acting between the universal wheels 1 ~ 4 and the ground. The signal-to-noise ratios of the RSM are 62.042, 41.058, 214.485, and 53.08, respectively. This indicates that the RSM has a high resolution and can be used to fit the maximum contact force acting between the universal wheels 1 ~ 4 and the ground. That is, the RSM can be used for the correlation analysis and prediction of the maximum contact force under this condition.

The variation coefficients of each RSM are 1.2%, 1.59%, 0.26%, and 0.64%. The fitting degree of all the equations meets the requirements, the model has a high adaptability, each response surface function can better represent the maximum contact force of the robot between the wheel and the ground, and the RSM has a high reliability. Finally, the differences between *Adj* R^2 and *Pred* R^2 in the function are 0.0413, 0.0887, 0.0026, and 0.0472, while each difference is less than 0.2, which indicates that the RSM does not need to be further optimized.

Table 4 Statistical analysis of errors in regression equation *M*

Source	Result	Source	Result
Std. Dev.	0.15	R^2	0.9941
Mean	159.89	*Adj* R^2	0.9865
C.V. %	0.096	*Pred* R^2	0.9789
PRESS	0.59	*Adeq Precision*	35.313

Table 5 Statistical analysis of errors in regression equation Y_1

Source	Result	Source	Result
Std. Dev.	3.92	R^2	0.9970
Mean	325.59	*Adj* R^2	0.9931
C.V. %	1.20	*Pred* R^2	0.9518
PRESS	1723.41	*Adeq Precision*	62.042

Table 6 Statistical analysis of errors in regression equation Y_2

Source	Result	Source	Result
Std. Dev.	4.21	R^2	0.9935
Mean	265.16	*Adj* R^2	0.9852
C.V. %	1.59	*Pred* R^2	0.8965
PRESS	1984.88	*Adeq Precision*	41.058

Table 7 Statistical analysis of errors in regression equation Y_3

Source	Result	Source	Result
Std. Dev.	0.61	R^2	0.9998
Mean	232.06	*Adj* R^2	0.9996
C.V. %	0.26	*Pred* R^2	0.9970
PRESS	42.05	*Adeq Precision*	214.485

Table 8 Statistical analysis of errors in regression equation Y_4

Source	Result	Source	Result
Std. Dev.	1.07	R^2	0.9966
Mean	167.92	*Adj* R^2	0.9921
C.V. %	0.64	*Pred* R^2	0.9449
PRESS	128.13	*Adeq Precision*	53.08

According to the normal probability distribution diagram of the RSM (*M*) presented in Figure 5 (a), the residual points of *M* are evenly and compactly distributed near the straight line. This indicates that the fitting effect of the objective function RSM is accurate [29]. According to the residual distribution diagram of the RSM (*M*) presented in Figure 5 (b), the studentized residual points of the objective function are discrete and randomly distributed on both sides of the horizontal line with a residual error of 0, narrow distribution range, and relatively uniform distribution. This proves that the objective function of the RSM is highly reliable.

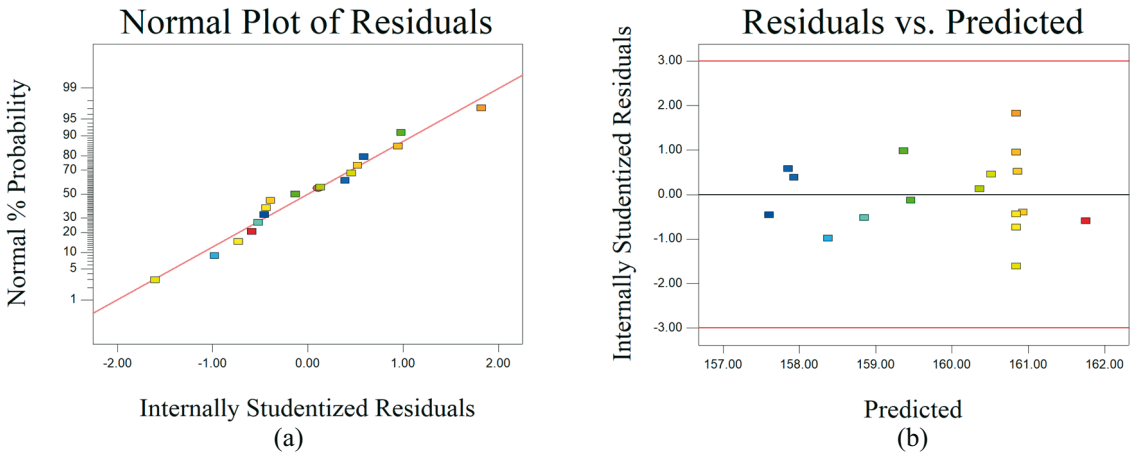

Fig. 5 RSM *M* (a) normal probability distribution diagram (b) residual distribution diagram

According to the normal probability distribution of the RSM with respect to the constraint functions Y_1, Y_2, Y_3, and Y_4 presented in Figures 6 (a)-(d), all residual points are close to the straight line, which indicates that the fitting effect of the RSM with the constraint function is better. According to the residual distribution diagram of the RSM with respect to the constraint functions Y_1, Y_2, Y_3, and Y_4 presented in Figure 7 (a)-(d), all studentized residual points are discrete and randomly distributed on both sides of the horizontal line with a residual error of 0, which is relatively uniform. This proves that the reliability of each constraint function of the RSM is high.

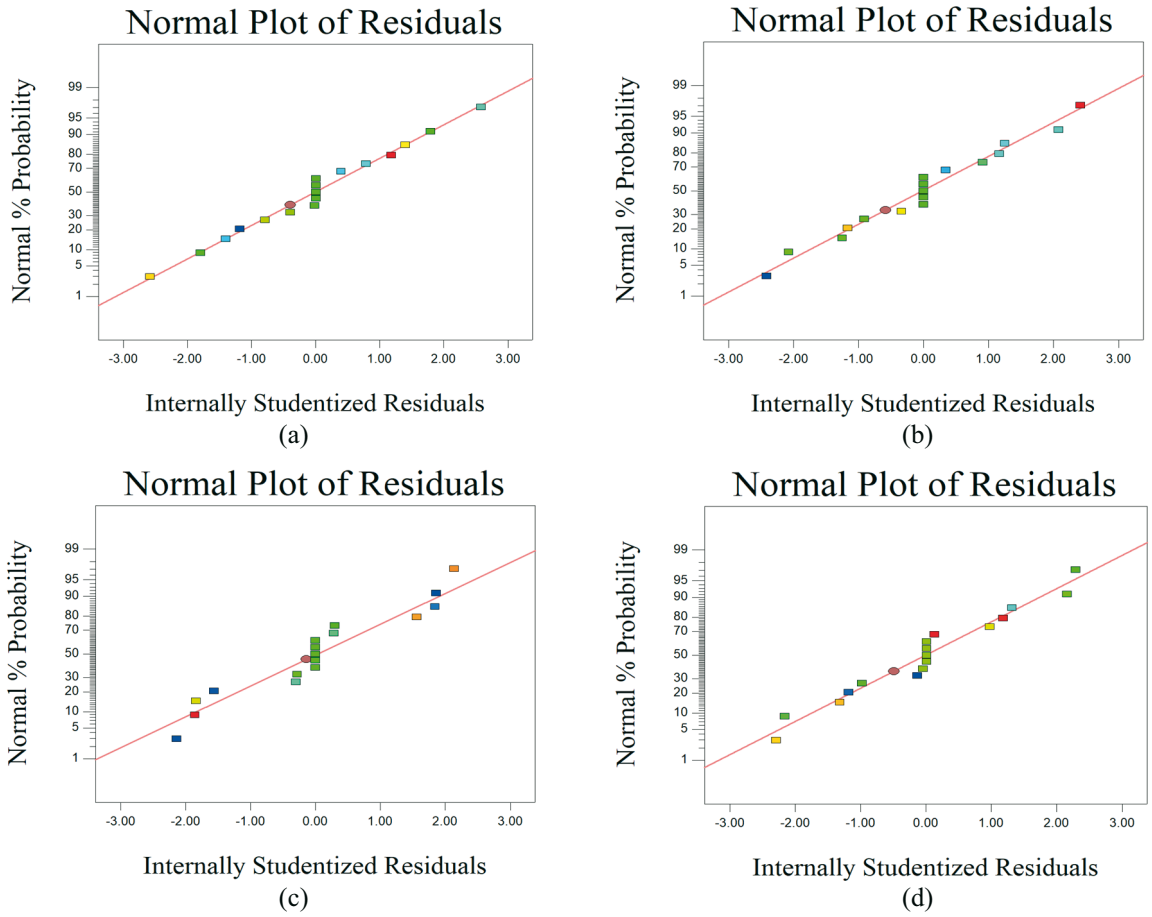

Fig. 6 Normal probability distribution diagram of RSM with respect to constraint functions (a) Y_1, (b) Y_2, (c) Y_3 and (d) Y_4

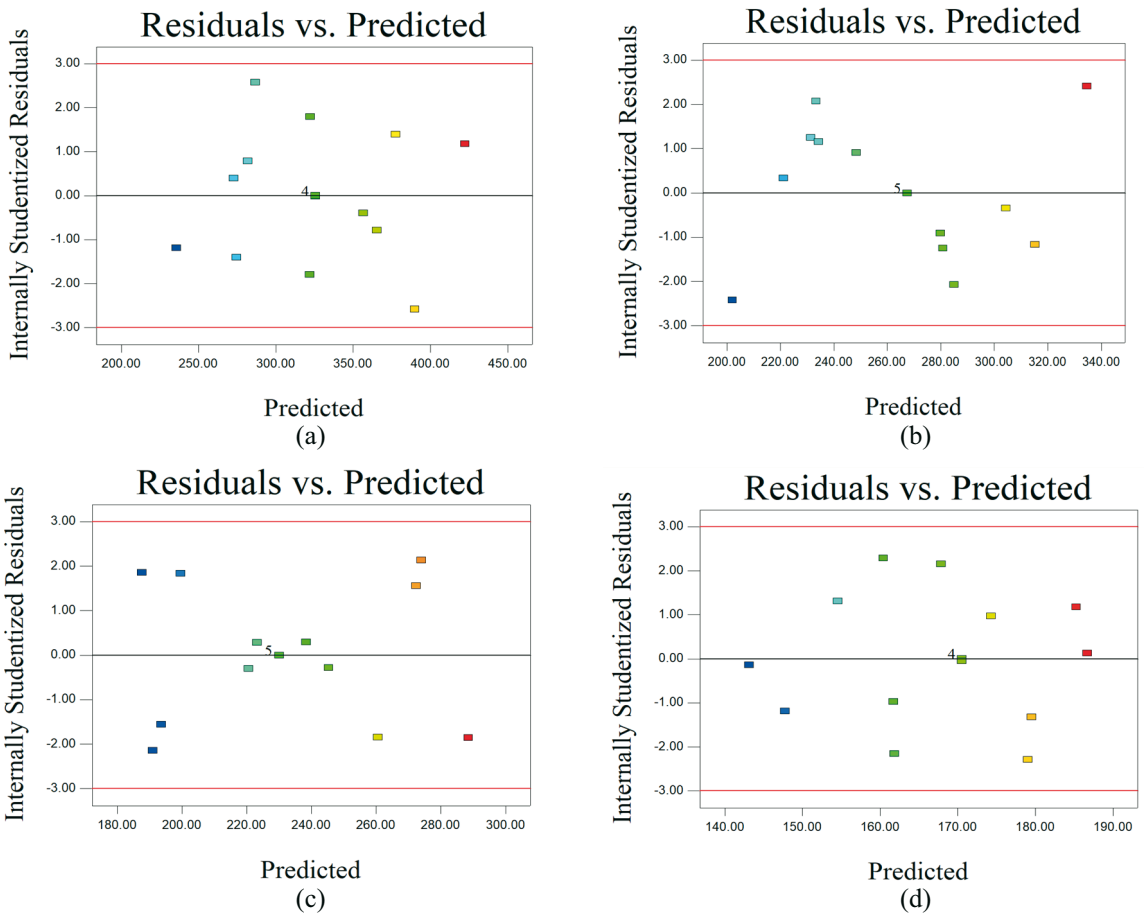

Fig. 7 Residual distribution diagram of RSM with respect to constraint functions (a) Y_1, (b) Y_2, (c) Y_3 and (d) Y_4

3.4 Validation of the RSM

In order to judge the rationality and correctness of the developed RSM, two evaluation indexes (*Adj* R^2 and *Pred* R^2) are used to verify its fitting accuracy. The value range of these two evaluation indices is [0,1]. A calculation result close to 1 indicates a high fitting accuracy of the established RSM and an accurate final result. The values of the design variables are substituted into the RSM to obtain the response values of each fitting function. Figures 8 and 9 present the error scatter plots between the predicted values of each RSM and the test values. Because the slope of the straight line $y = x$ is 1, the closer the scatter points to the straight line, the more uniform the distribution. This indicates that the smaller the error between the data, the higher the accuracy of the final RSM and the smaller the error between the predicted value and the experimental value. The error scatter diagram of the objective function M is illustrated in Figure 8. It can be seen that the error scatter points of M are relatively concentrated. In the analysed error scatter points, all points are close to the straight line and only few points are distributed outside the straight line, however, still very close to it. Moreover, almost all the other scatter points are distributed on the straight line, which indicates that the fitting accuracy of the RSM of the objective function M is high.

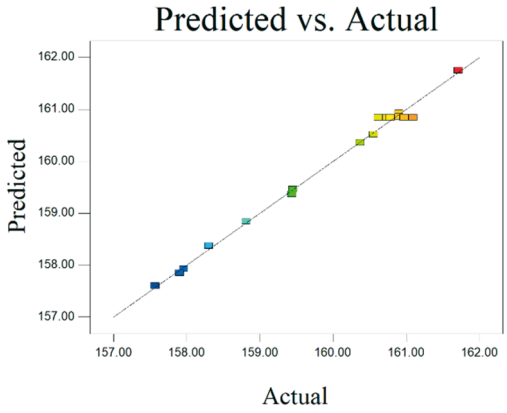

Fig. 8 Error scatter diagram of objective function *M* of RSM

It can be seen from Figure 9 (a) that the error scatter points of Y_1 are relatively uniform and scattered. However, the distance from the straight line is very small, which indicates that the fitting accuracy of the Y_1 RSM is high. It can be seen from Figure 9 (b) that the error scatter points of Y_2 are relatively concentrated. Among the analysed error scatter points, three are distributed outside the straight line, however, still very close to it. Almost all other scatter points are distributed on the straight line, which indicates that the fitting accuracy of the Y_2 RSM is very high. It can be observed from Figure 9 (c) that the concentration effect of each error scatter point of Y_3 is the best. In addition, all error scatter points are distributed on the straight line with uniform distribution, which indicates that the accuracy of the developed Y_3 RSM is very high. It can be seen from Figure 9 (d) that the error scatter points of Y_4 are evenly distributed on both sides of the straight line and very close to the straight line. Some points are distributed on the straight line, which indicates that the fitting accuracy of the Y_4 RSM is high. The values of the evaluation indices of each RSM are close to 1, which indicates that the accuracy of the RSM can meet the requirements.

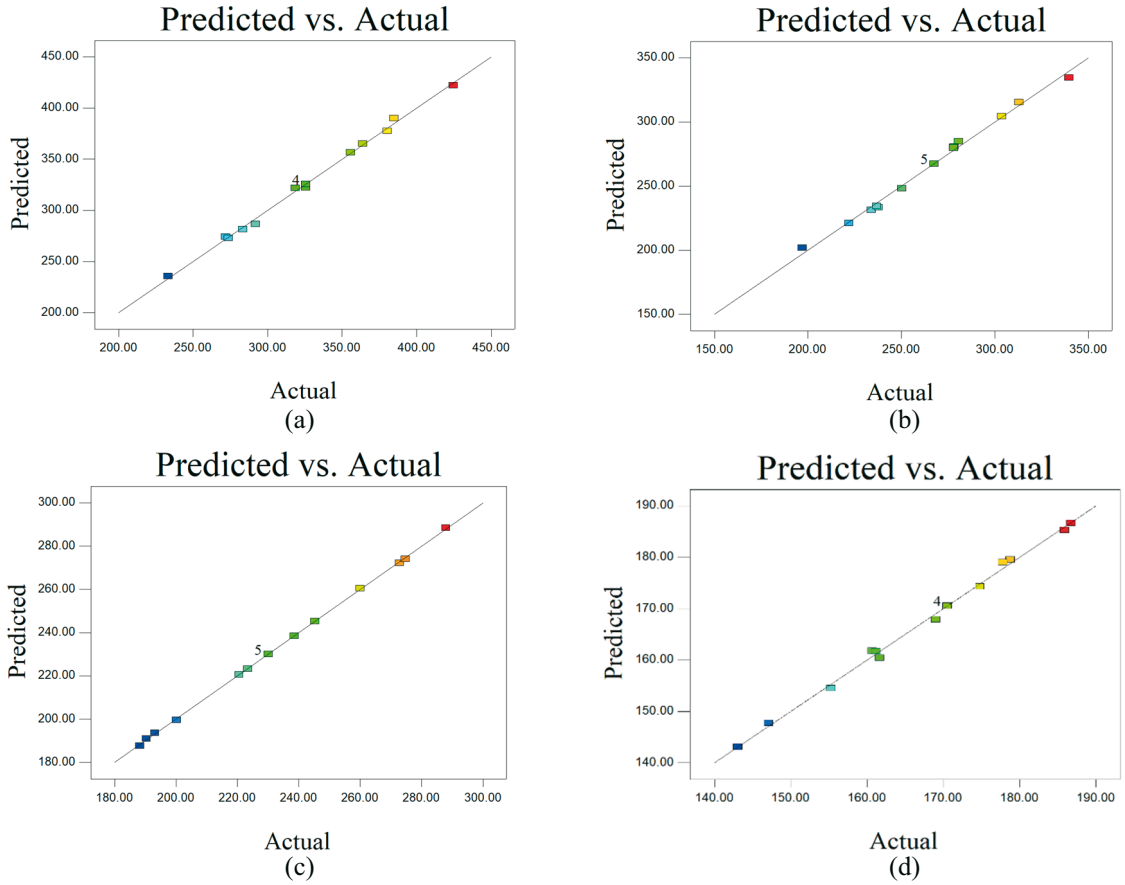

Fig. 9 Error scatter diagram of RSM constraint functions (a) Y_1, (b) Y_2, (c) Y_3 and (d) Y_4

3.5 Influence of the interaction between design variables on the objective function

Figures 10, 11, and 12 present the response surface diagrams of the interaction between the robot mass, the patient weight, the elastic coefficient and the objective function. Note that the greater the slope angle and the darker the colour of the surface response diagram, the more significant the interaction between the design variables and the greater the impact on the objective function. It can be seen from Figure 10 that, during the interaction between the robot mass and patient weight, when the elastic coefficient x_3 = 3 N/mm, the objective function value (M) first increases and then decreases with the increase of x_1 and x_2. When the weight of the rehabilitation robot is 100 ~ 125 kg and the patient's weight is 65 ~ 95 kg, the rehabilitation robot has the best stability. It can be seen from Figure 11 that during the interaction between the robot mass and the elastic coefficient, when the patient's weight x_2 = 75 kg, the objective function value (M) decreases with the increase of x_1. However, it gradually increases with the increase of x_3. It can be seen that the increase in the elastic coefficient has a high impact on the robot stability, when the patient's weight remains unchanged. The rehabilitation robot has the best stability when its mass is 100 ~ 120 kg and the elastic coefficient is 3 ~ 4 N/mm. It can be seen from Figure 12 that during the interaction between the patient's weight and the elastic coefficient, when the robot mass x_1 = 125 kg, the objective function value (M) first increases and then decreases with the increase of x_2 and x_3. Assuming that the robot mass remains unchanged, the patient's weight and the elastic coefficient have a high impact on the robot stability in the middle and upper region. The robot has the best stability when the patient's weight is 65 ~ 80 kg and the elastic coefficient is 3.5 ~ 4 N/mm.

The mathematical model developed using the Box-Behnken statistical method is completed by analysing the regression model equation and the response surface. The optimal conditions for the stability of the robot are determined, based on the previously mentioned response surface approximate function. The robot mass is 126 kg, the patient weight is less than or equal to 75 kg, and the elastic coefficient is 4 N/mm.

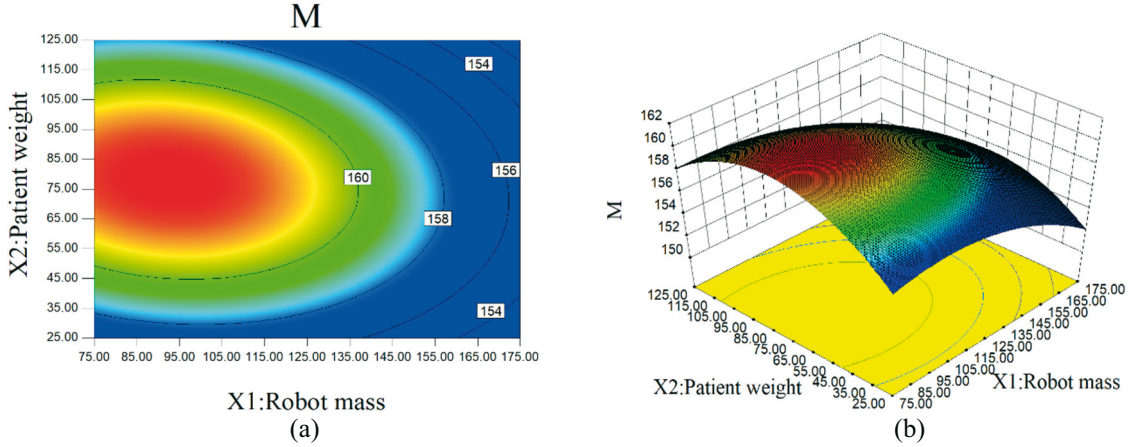

(a) (b)

Fig. 10 Contour map (a) and three-dimensional response surface map (b) of objective function M with respect to variables x_1 and x_2

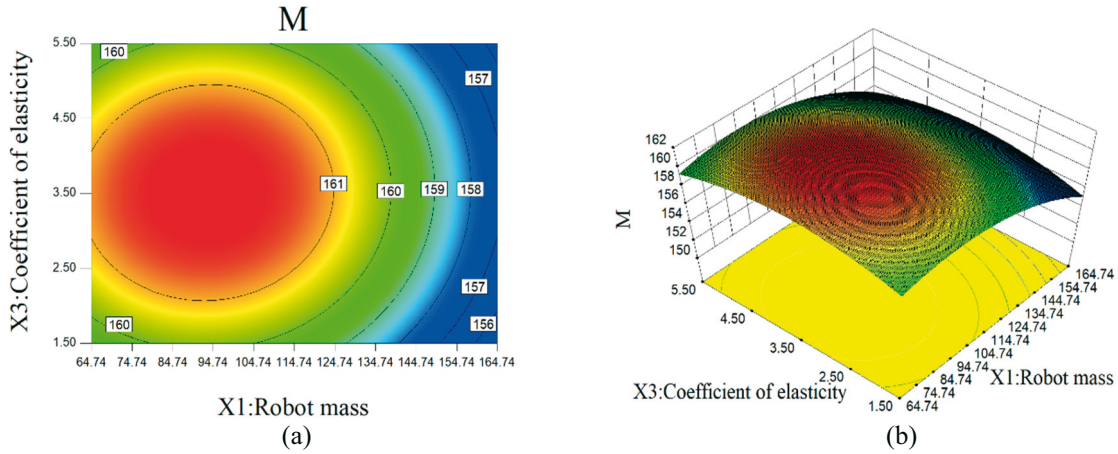

Fig. 11 Contour map (a) and three-dimensional response surface map (b) of objective function M with respect to variables x_1 and x_3

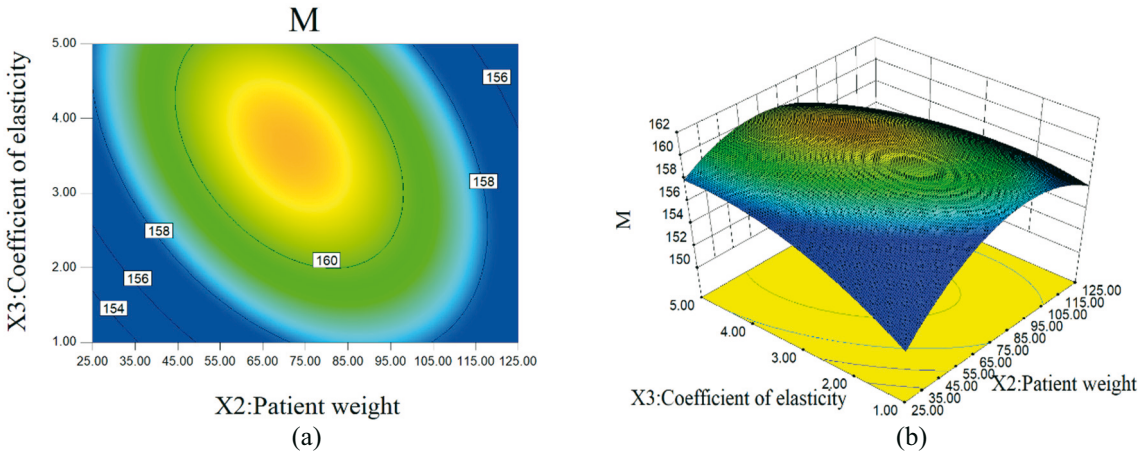

Fig. 12 Contour map (a) and three-dimensional response surface map (b) of objective function M with respect to variables x_2 and x_3

4. Rehabilitation robot steering error and stability experiments

4.1 Steering error experiment

An experimental prototype of the rehabilitation robot is built with a mass of 130 kg and an experimental platform for testing the steering error of the robot is developed, as shown in Figure 13. The central point of the axis of the driving wheels O_5 and O_6 of the robot prototype is set as the sampling mark point. The plane coordinate value of the sampling mark point before the prototype turns in place, is set to (0,0). The driving wheels O_5 and O_6 of the prototype are then controlled to move at the same speed and in the opposite direction of rotation and to stop after the robot rotates for one circle. Afterwards, the new coordinates of the sampling mark point are recorded as (X, Y). The steering error experiment is repeated 12 times. The new coordinate values of 12 sampling marker points are recorded. The kinematic control method of the rehabilitation robot is presented in more detail in Appendix A. The new coordinate value data of the sampling mark points are presented in Table 9. In addition, the displacement changes curve of the central point of the robot prototype, in the X and Y axes of the plane coordinates, is drawn according to Table 9. The curve presenting the experimental results for the robot steering error is illustrated in Figure 14.

(a) (b)

Fig. 13 Experimental platform for testing the steering error of the rehabilitation robot

Table 9 Experimental data of the dexterity error of the rehabilitation robot

Num	1	2	3	4	5	6	7	8	9	10
X	31	45	40	52	37	53	55	40	39	35
Y	-15	-16	-18	-16	-13	-19	-14	-19	-20	-17

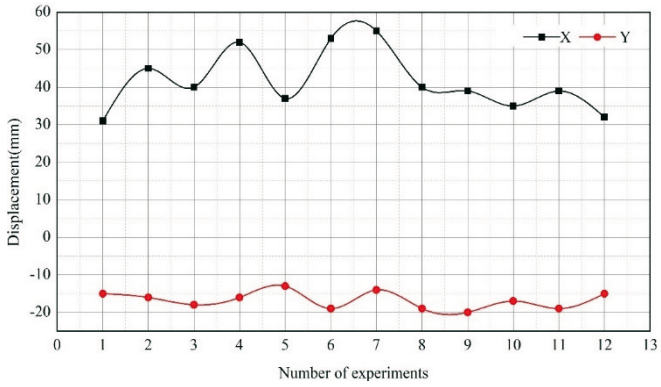

Fig. 14 Experimental results for the robot steering error

According to the experimental data of the robot steering error, the maximum error of the small radius steering of the rehabilitation robot in the X-direction is 55 mm, the minimum error is 31 mm, the maximum error in the Y-direction is 20 mm, and the minimum error is 13 mm, which is relatively small compared to the robot base size of 1,025 mm × 880 mm. The experimental results demonstrate that the prototype is flexible in steering and can move in a narrow space, thus meeting the design requirements.

4.2 Robot stability experiments

In order to accurately judge the stability effect of the robot under the optimal conditions, a membrane pressure sensor is mounted between the prototype wheel and the ground. The change in the contact force acting between the robot wheel and the ground is transmitted to the upper computer through the pressure sensor transmission module. The stability effect of the robot is then objectively and quantitatively evaluated according to the contact force change. Note that an IMS-C40A membrane pressure sensor is used. This sensor has a sensitivity of 20 N and range of 0 ~ 1500 N. Then, a volunteer of 175 cm height and 75 kg weight is selected. The auxiliary force is quantitatively adjusted by the force sensor feedback data of the robot weight support balance system, so that the value of the weight support of the robot to the volunteer is 300 N, and the volunteer is in a state of body balance. In this state, the volunteer chooses any posture to fall, and the pressure sensor collects the changes in the indirect contact force acting between the wheel and the ground and sends it back to the upper computer. Based

on these experimental requirements, the stability test platform of the robot and the arrangement of the membrane pressure sensor are built, as shown in Figure 15. The multi-condition experiment of the rehabilitation robot stability is shown in Figure 16.

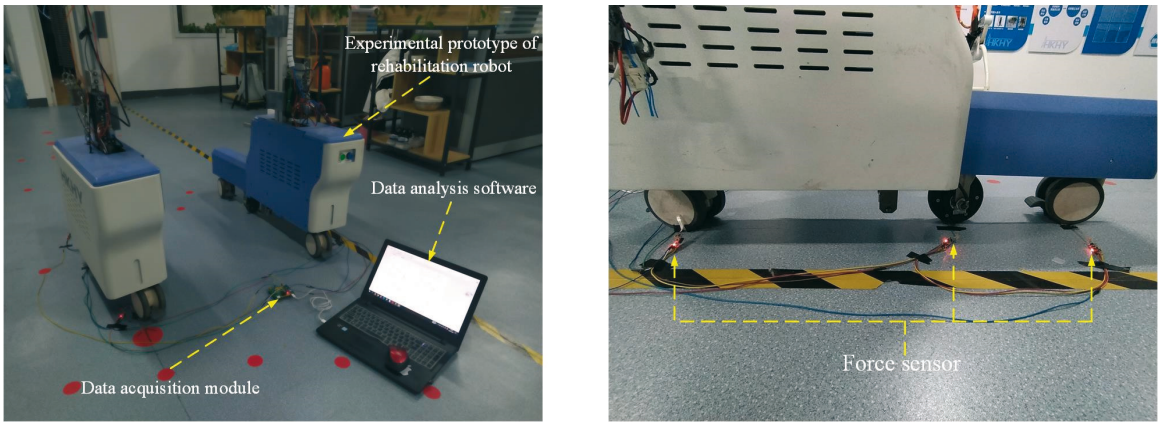

(a) (b)

Fig. 15 Rehabilitation robot (a) stability experimental platform and (b) layout of membrane pressure sensor

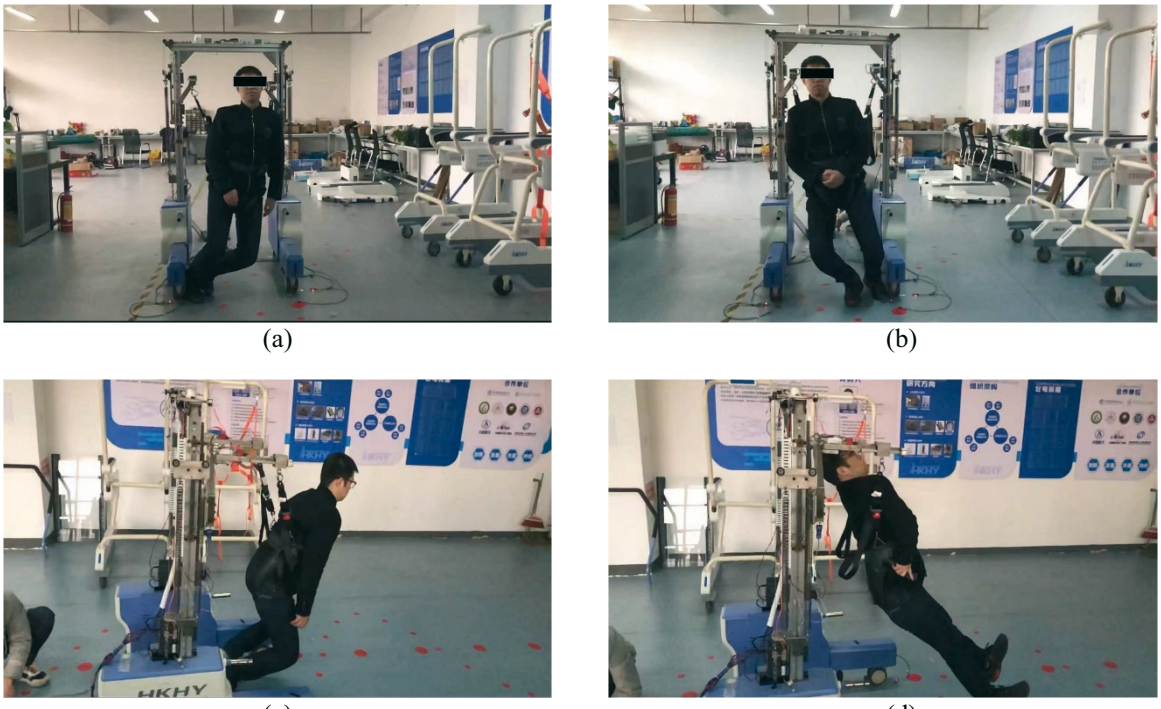

(a) (b)

(c) (d)

Fig. 16 Multi-condition experiment of robot stability (a) left fall (b) right fall (c) forward fall (d) backward fall

The experimental study was performed on the rehabilitation robot stability test platform built in Figure 15. The membrane pressure sensor uploads the collected contact force acting between the robot wheel and the ground to the upper computer. After the experiment, the force curve is drawn according to the data about the contact force acting between each wheel and the ground, as shown in Figures 17-24.

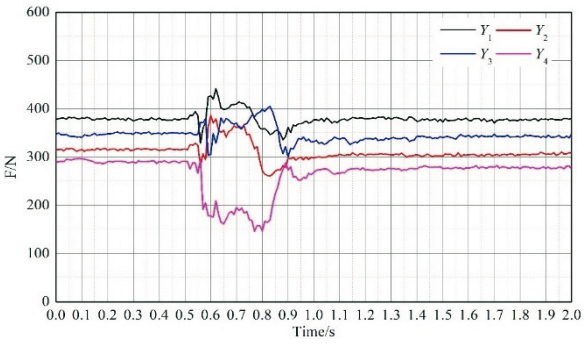

Fig. 17 Contact force variation curves of robot universal wheels O_1, O_2, O_3, and O_4 and the ground, under left impact

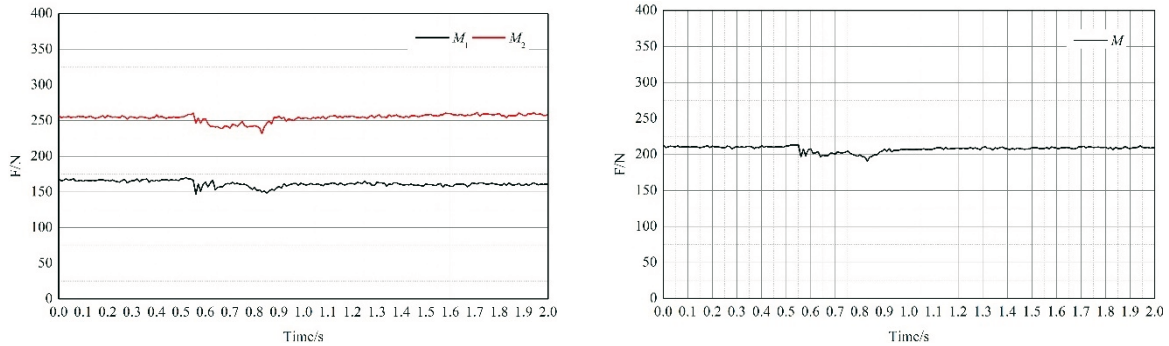

(a) (b)

Fig. 18 Contact force variation curves of robot driving wheels (a) O_5 and (b) O_6 and the ground, under left impact

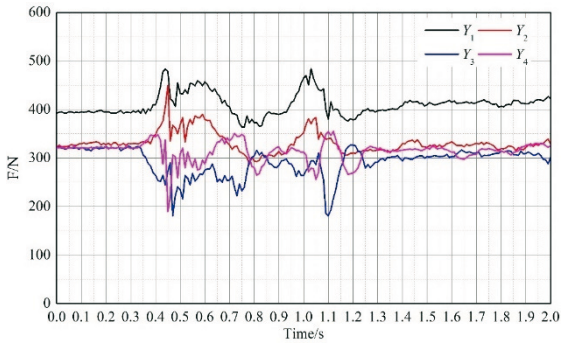

Fig. 19 Contact force variation curves of robot universal wheels O_1, O_2, O_3, and O_4 and the ground, under right impact

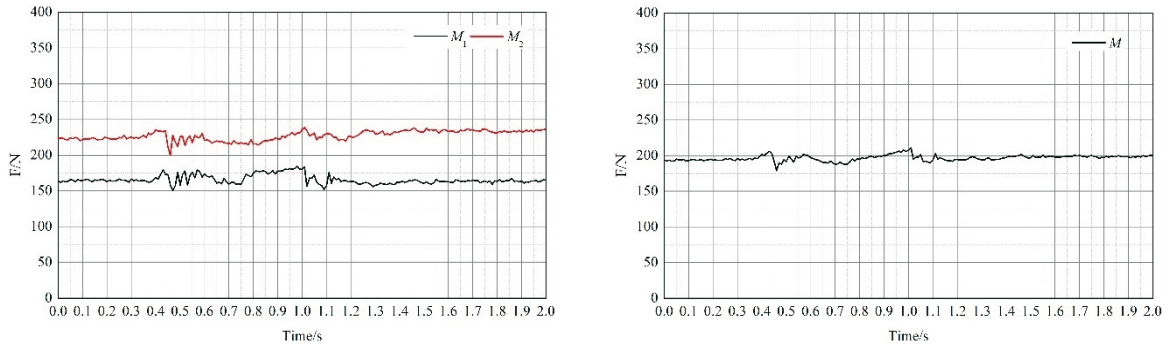

(a) (b)

Fig. 20 Contact force variation curves of robot driving wheels (a) O_5 and (b) O_6 and the ground, under right impact

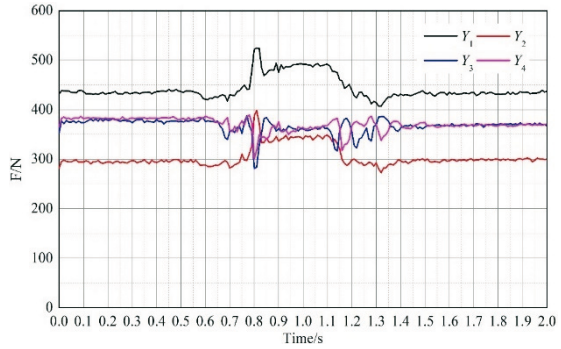

Fig. 21 Contact force variation curves of robot universal wheels O_1, O_2, O_3, and O_4 and the ground, under back impact

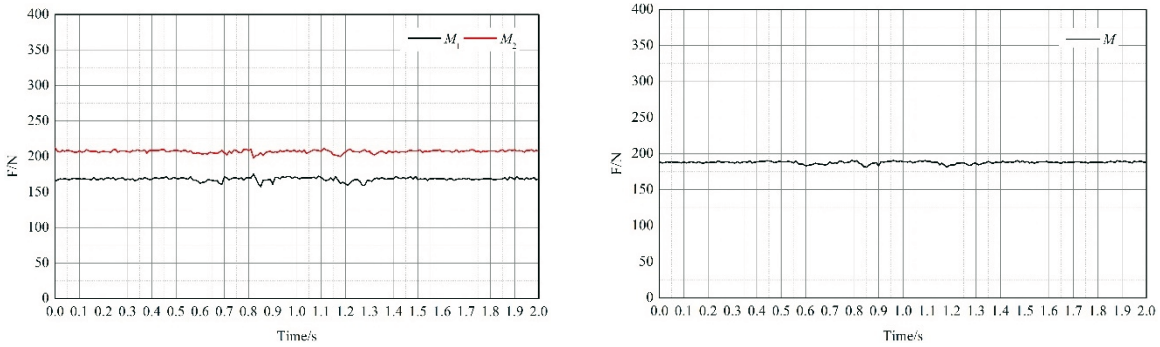

(a) (b)

Fig. 22 Contact force variation curves of robot driving wheels (a) O_5 and (b) O_6 and the ground, under back impact

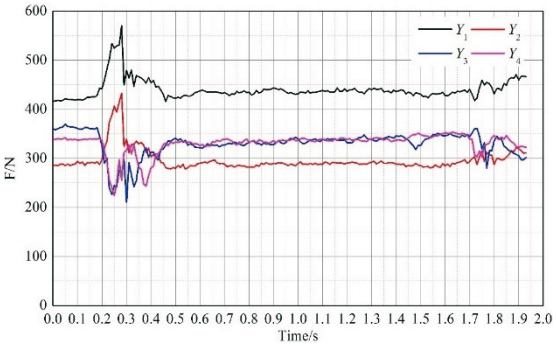

Fig. 23 Contact force variation curves of robot universal wheels O_1, O_2, O_3, and O_4 and the ground, under forward impact

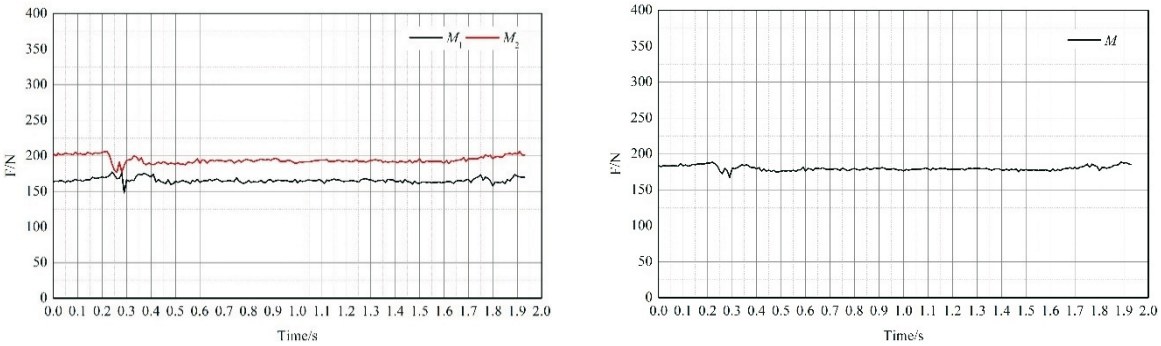

(a) (b)

Fig. 24 Contact force variation curves of robot driving wheels (a) O_5 and (b) O_6 and the ground, under forward impact

According to the diagram of the rehabilitation robot structure, Figure 4, the wheels O_1 and O_3 are located on the left side, while the wheels O_2 and O_4 are located on the right side of the robot. The Y_1, Y_2, Y_3, and Y_4 curves represent the contact force acting between the wheels O_1, O_2, O_3, and O_4 and the ground, respectively. According to the contact force variation curves of the robot universal wheels presented in Figures 17, 19, 21, and 23, when the volunteers fall to the left, right, backwards, and forwards, respectively, the contact force acting between the robot universal wheels and the ground suddenly changes. During the volunteers' fall, the contact force acting between the rehabilitation robot wheels O_1 and O_2, O_3, and O_4 and the ground has the same trend of change. However, the trend of change of the force on the front and rear wheels is opposite. The robot increases the force on the front wheels and decreases the force on the rear wheels. This is due to the fact that the centre of gravity of the robot moves forward after the volunteers fall. When the volunteers fall to the left, the minimum contact forces acting between the robot wheels O_1 and O_3 and the ground are 338.61 N and 223.77 N, respectively, and the minimum contact forces acting between the wheels O_2 and O_4 and the ground are 271.10 N and 179.18 N, respectively. When the volunteers fall to the right, the minimum contact forces acting between the robot wheels O_1 and O_3 and the ground are 363.31 N and 180.81 N, respectively, and the minimum contact forces acting between the wheels O_2 and O_4 and the ground are 287.17 N and 189.57 N, respectively. When tilting backwards and falling, the minimum contact forces acting between the robot wheels O_1 and O_3 and the ground are 407.07 N and 281.05 N, respectively, and the minimum contact forces acting between the wheels O_2 and O_4 and the ground are 272.71 N and 300.69 N, respectively. When falling forwards, the minimum contact forces acting between the robot wheels O_1 and O_3 and the ground are 416.04 N and 210.71 N, respectively, and the minimum contact forces acting between the wheels O_2 and O_4 and the ground are 278.16 N and 224.32 N, respectively. The values of the contact force acting between the robot wheels and the ground are greater than 0 N, which indicates that the robot body is still in a stable state, despite the shaking trend. In Figures 18, 20, 22, and 24, M_1 is the maximum contact force acting between the driving wheel O_5 of the rehabilitation robot and the ground, M_2 is the maximum contact force acting between the driving wheel O_6 and the ground, and the objective function M is the average value of M_1 and M_2. It can be seen from the curves presenting the variation of the contact force acting between the driving wheels and the ground given in Figures 18, 20, 22, and 24 that, when the robot body is in a stable state, the contact force acting between the driving wheels on the left and right sides and the ground remains unchanged, and the contact force is 190 N. During the fall of the volunteers to the left side, the minimum contact force acting between the driving wheel and the ground is 148.61N. During the fall to the right side, the minimum contact force acting between the driving wheel and the ground is 150.73 N. During the backward fall, the minimum contact force acting between the driving wheel and the ground is 149.87 N. During the forward fall, the minimum contact force acting between the driving wheel and the ground is 148.18 N and finally, the contact force acting between the driving wheel and the ground gradually tends to be stable. According to the variation characteristics of the contact force acting between the robot wheel and the ground presented in Figures 17-24, the robot can continue to maintain a stable state under the action of a lateral external force. According to the experimental results of the rehabilitation robot affected by external forces in four different directions, it can be deduced that the structural design of the robot based on the optimal stability parameters is reasonable and reliable.

5. Conclusions

With the aim of responding to the demands of stroke patients for rehabilitation therapy, this paper proposes and designs a lower limb rehabilitation training robot for stroke patients. First, the mechanical structural design and the working principle of the rehabilitation robot are

introduced. The overall design of the robot can assist the patients to stand and walk on the ground, reduce the walking burden of the patients' lower limbs, and promote the lower limb rehabilitation training and daily walking of stroke patients. In addition, with the help of rehabilitation robots, physiotherapists no longer need to rely on their own strength to assist patients in their rehabilitation training, which greatly reduces the burden on them. Physiotherapists can also focus more on guiding patients in the rehabilitation training and correcting patients' wrong gait. Based on the wheel configuration scheme of the rehabilitation robot, its motion characteristics are analysed and the relationship between its wheel motion parameters and posture is obtained. The steering error experiment of the prototype demonstrates that the maximum errors of the robot in the X and Y directions are 55 mm and 20 mm, respectively. The experimental results show that the rehabilitation robot can flexibly turn and move in a narrow space, which meets the design requirements. Based on the response surface method, the second-order RSM of the rehabilitation robot stability with respect to the influencing parameters x_1, x_2, and x_3, is developed. Through a series of deterministic experiments, the stability mathematical model of the rehabilitation robot is approximated with a polynomial function, and the stability limit state function of the rehabilitation robot is obtained. The fitting degree of the objective function regression model is 99.41%, while that of the constraint function regression model is 99.70%, 99.35%, 99.98% and 99.66%. The residual distribution and error scatter diagram prove that the model has high reliability and fitting accuracy. By analysing the contour map and the three-dimensional response surface map of the objective function, it can be deduced that the interaction between the design variables x_1, x_2, and x_3 has a high impact on the value and trend of change of the objective function. Based on the approximate function, the optimal parameter combination of the stability of the rehabilitation robot is obtained. More precisely, the robot mass is 130 kg, the patient's weight is less than or equal to 75 kg and the elastic coefficient is 4 N/mm. It is verified by experiments that, when volunteers fall in any direction, the contact force acting between the driving wheel and the ground of the robot changes considerably. The trend of change in the contact force between the wheels on different sides of the robot is opposite, and the contact force presents an alternating trend of change. The values of the contact force acting between the robot wheel and the ground are greater than 0 N, which indicates that the wheels are in contact with the ground and do not leave the ground. This shows that although the robot body has a shaking trend, it is still in a stable state. Finally, the minimum contact force acting between the driving wheel and the ground is almost 190 N, which indicates that the rehabilitation robot gradually tends to reach a stable state. The correctness of the method of optimization analysis of the stability parameters of the rehabilitation robot proposed in this paper is proved, which means that a research method is provided for the follow-up study to optimize the parameters of the stability of the robot structure, reduce the design redundancy, and improve the design efficiency of the robot.

REFERENCES

[1] Johnson, C.O.; Minh, N.; Roth, G.A.; Nichols, E.; Alam, T.; Abate, D.; Abd-Allah, F.; Abdelalim, A.; Abraha, H.N.; Abu-Rmeileh, N.M., et al. Global, regional, and national burden of stroke, 1990-2016: a systematic analysis for the Global Burden of Disease Study 2016. *Lancet Neurology* **2019**, *18*, 439-458. https://doi.org/10.1016/S1474-4422(19)30034-1

[2] Hobbs, B.; Artemiadis, P. A Review of Robot-Assisted Lower-Limb Stroke Therapy: Unexplored Paths and Future Directions in Gait Rehabilitation. *Frontiers in Neurorobotics* **2020**, *14*. https://doi.org/10.3389/fnbot.2020.00019

[3] Gittler, M.; Davis, A.M. Guidelines for Adult Stroke Rehabilitation and Recovery. *Jama-Journal of the American Medical Association* **2018**, *319*, 820-821. https://doi.org/10.1001/jama.2017.22036

[4] Benjamin, E.J.; Muntner, P.; Alonso, A.; Bittencourt, M.S.; Callaway, C.W.; Carson, A.P.; Chamberlain, A.M.; Chang, A.R.; Cheng, S.; Das, S.R. Heart disease and stroke statistics—2019 update: a report from the American Heart Association. *Circulation* **2019**, *139*, e56-e528.

[5] Cespedes, N.; Munera, M.; Gomez, C.; Cifuentes, C.A. Social Human-Robot Interaction for Gait Rehabilitation. *Ieee Transactions on Neural Systems and Rehabilitation Engineering* **2020**, *28*, 1299-1307. https://doi.org/10.1109/TNSRE.2020.2987428

[6] Udupa, S.; Kamat, V.R.; Menassa, C.C. Shared autonomy in assistive mobile robots: a review. *Disability and Rehabilitation: Assistive Technology* **2021**, 1-22. https://doi.org/10.1080/17483107.2021.1928778

[7] Shi, D.; Zhang, W.; Zhang, W.; Ding, X. A Review on Lower Limb Rehabilitation Exoskeleton Robots. *Chinese Journal of Mechanical Engineering* **2019**, *32*, 1-11. https://doi.org/10.1186/s10033-019-0389-8

[8] Leme, B.; Hirokawa, M.; Kadone, H.; Suzuki, K. A Socially Assistive Mobile Platform for Weight-Support in Gait Training. *International Journal of Social Robotics* **2021**, *13*, 459-468. https://doi.org/10.1007/s12369-019-00550-x

[9] Catalan, J.M.; Blanco, A.; Bertomeu-Motos, A.; Garcia-Perez, J.V.; Almonacid, M.; Puerto, R.; Garcia-Aracil, N. A Modular Mobile Robotic Platform to Assist People with Different Degrees of Disability. *Applied Sciences-Basel* **2021**, *11*. https://doi.org/10.3390/app11157130

[10] Yan, Q.; Huang, J.; Yang, Z.; Hasegawa, Y.; Fukuda, T. Human-Following Control of Cane-Type Walking-Aid Robot Within Fixed Relative Posture. *IEEE/ASME Transactions on Mechatronics* **2021**, *PP*, 1-1. https://doi.org/10.1109/TMECH.2021.3068138

[11] Lee, L.-W.; Li, I.; Liang, T.-W. A Proof of Concept Study for the Design, Manufacturing, and Control of a Mobile Overground Gait-Training System. *International Journal of Fuzzy Systems* **2021**, *23*, 2396-2416. https://doi.org/10.1007/s40815-021-01051-8

[12] Martinez-Hernandez, U.; Dehghani-Sanij, A.A. Probabilistic identification of sit-to-stand and stand-to-sit with a wearable sensor. *Pattern Recognition Letters* **2019**, *118*, 32-41. https://doi.org/10.1016/j.patrec.2018.03.020

[13] Lanini, J.; Razavi, H.; Urain, J.; Ijspeert, A. Human intention detection as a multiclass classification problem: Application in physical human–robot interaction while walking. *IEEE Robotics and Automation Letters* **2018**, *3*, 4171-4178. https://doi.org/10.1109/LRA.2018.2864351

[14] Martinez-Hernandez, U.; Dehghani-Sanij, A.A. Adaptive Bayesian inference system for recognition of walking activities and prediction of gait events using wearable sensors. *Neural Networks* **2018**, *102*, 107-119. https://doi.org/10.1016/j.neunet.2018.02.017

[15] Lin, K.; Li, Y.; Sun, J.; Zhou, D.; Zhang, Q. Multi-sensor fusion for body sensor network in medical human–robot interaction scenario. *Information Fusion* **2020**, *57*, 15-26. https://doi.org/10.1016/j.inffus.2019.11.001

[16] Liu, Y.-X.; Wang, R.; Gutierrez-Farewik, E.M. A muscle synergy-inspired method of detecting human movement intentions based on wearable sensor fusion. *IEEE Transactions on Neural Systems and Rehabilitation Engineering* **2021**, *29*, 1089-1098. https://doi.org/10.1109/TNSRE.2021.3087135

[17] Zhou, J.; Yang, S.; Xue, Q. Lower limb rehabilitation exoskeleton robot: A review. *Advances in Mechanical Engineering* **2021**, *13*. https://doi.org/10.1177/16878140211011862

[18] Cai, S.; Bao, G.; Ma, X.; Wu, W.; Bian, G.-B.; Rodrigues, J.J.P.C.; de Albuquerque, V.H.C. Parameters optimization of the dust absorbing structure for photovoltaic panel cleaning robot based on orthogonal experiment method. *Journal of Cleaner Production* **2019**, *217*, 724-731. https://doi.org/10.1016/j.jclepro.2019.01.135

[19] Hu, M.; Wang, H.; Pan, X. Multi-objective global optimum design of collaborative robots. *Structural and Multidisciplinary Optimization* **2020**, *62*, 1547-1561. https://doi.org/10.1007/s00158-020-02563-x

[20] Liu, K.; Ji, S.; Sun, Z.; Xu, H.; Liu, Y. Structural design and optimization of bionic rehabilitation robot. *Journal of Jilin University. Engineering and Technology Edition* **2020**, *50*, 1144-1152.

[21] Petrović, N.; Marjanović, V.; Kostić, N.; Marjanović, N.; Dragoi, M.V. Means and Effects of Constraining the Number of Used Cross-Sections in Truss Sizing Optimization. *Transactions of FAMENA* **2020**, *44*, 35-46. https://doi.org/10.21278/TOF.44303

[22] Zdravković, M.; Korunović, N. Novel methodology for real-time structural analysis assistance in custom product design. *Facta Universitatis, Series: Mechanical Engineering* **2021**.

[23] Ramesh Kumar, A.; Jayabal, S.; Pradeep Kumar, M.; Thirumal, P. A Qualitative Analysis of Indoor Air Quality Pollutants inside a Private Car Cabin Using Response Surface Methodology. Transactions of FAMENA 2022, 46, 41-55. https://doi.org/10.21278/TOF.461017020

[24] Zhou, J.; Gao, J.; Wang, K.; Liao, Y. Design optimization of a disc brake based on a multi-objective optimization algorithm and analytic hierarchy process method. Transactions of FAMENA 2018, 42, 25-42. https://doi.org/10.21278/TOF.42403

[25] Miao, M.; Gao, X.; Zhu, W. A Construction Method of Lower Limb Rehabilitation Robot with Remote Control System. *Applied Sciences-Basel* **2021**, *11*. https://doi.org/10.3390/app11020867

[26] Dul, J.; deVlaming, P.M.; Munnik, M.J. A review of ISO and CEN standards on ergonomics. *International Journal of Industrial Ergonomics* **1996**, *17*, 291-297. https://doi.org/10.1016/0169-8141(95)00068-2

[27] Ma, C.; Wen, P.; Hu, J. Measurement of Human Body's Feature Dimensions Based On The National Standards. In Proceedings of 2nd International Conference on Advanced Design and Manufacturing Engineering (ADME 2012), Taiyuan, PEOPLES R CHINA, 2012, Aug 16-18; pp. 1525-+.

[28] He, W.; Dong, W.; Sun, L.; Meng, X.; Zhu, Y. Optimization on wear target parameters for gear shaft mold based on response surface method. *Forging & Stamping Technolog* **2020**, *45*, 166-170.

[29] Kallath, H.; Lee, J.S.; Kholi, F.K.; Ha, M.Y.; Min, J.K. A multi-objective airfoil shape optimization study using mesh morphing and response surface method. *Journal of Mechanical Science and Technology* **2021**, *35*, 1075-1086. https://doi.org/10.1007/s12206-021-0221-0

Submitted: 20.4.2022

Accepted: 31.8.2023

Xueshan Gao
Mingda Miao*
Pengfei Zhang
School of Mechatronic Engineering, Beijing Institute of Technology, Beijing 100081, China
Peng Zhao
School of Electrical Electronic & Computer Science, Guangxi University of Science and Technology, Liuzhou 545006, China
*Corresponding author: 845771325@qq.com

Appendix A

Kinematic analysis of the rehabilitation robot

The motion parameters and structural dimensions of the rehabilitation robot are simplified, as shown in Figure 1. In Figure 4, *XOY* represents the global coordinate system of the robot, *xpy* denotes its local coordinate system, *p* is the geometric centre point of its coaxial driving wheel which can be determined by *x* and *y* in the global coordinate system, θ is the included angle between the global coordinate system and the robot coordinate system, w_1 and w_2 represent the angular velocities of the driving wheels O_5 and O_6, respectively, *r* is the radius of the driving wheel, and 2*b* is its centre distance.

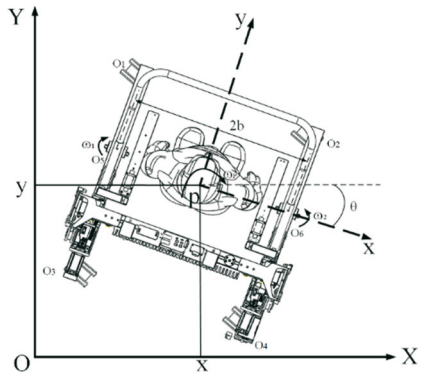

Fig. 4 Schematic diagram of structural dimensions of the robot

The motion of the robot driving wheel affects its position and attitude. Therefore, it is necessary to unify the motion speed and the direction of the robot driving wheel in the coordinate system, develop the conversion relationship between the global coordinate system and the local coordinate system of the robot, and analyse the influence of the motion parameters of the driving wheel on its position and attitude. In the local coordinate system, the rotation angular speeds of the left and right driving wheels of the robot are w_1 and w_2, respectively. Considering $V(t) = [v, w]^T$, where *v* and *w* represent the linear and the angular speed of the robot *p* point, respectively, the motion speed of the rehabilitation robot is expressed as:

$$V(t) = \begin{bmatrix} v \\ w \end{bmatrix} = \begin{bmatrix} \frac{r}{2} & \frac{r}{2} \\ \frac{r}{2b} & -\frac{r}{2b} \end{bmatrix} \begin{bmatrix} \varphi_l \\ \varphi_r \end{bmatrix} \tag{1}$$

According to the structural dimension diagram of the robot:

(1) when $v \neq 0$ and $w = 0$, the robot can perform linear motion;

(2) when $v = 0$ and $w \neq 0$, the robot rotates around the geometric centre *p* point;

To develop the mapping relationship between the motion parameters of the driving wheel and the posture of the robot, the kinematics model is idealized. That is, the geometric centre of the robot coincides with the centre of gravity, and the driving wheel meets the conditions of pure rolling and no sliding as follows:

$$\dot{x}\sin\theta - \dot{y}\cos\theta = 0 \tag{2}$$

The kinematic equation of the rehabilitation robot is given by the following equation:

$$\dot{q} = S(q)V(t) \tag{3}$$

where $S(q)=\begin{bmatrix}\cos\theta & 0\\ \sin\theta & 0\\ 0 & 1\end{bmatrix}$.

Note that $S(q)$ is a Jacobian matrix which converts the speed $V(t)$ of the robot in the local coordinate system into the speed $\dot{q}$ in the Cartesian coordinate system. The kinematic equation of the two-wheel differential drive rehabilitation robot is given as follows:

$$\dot{q}=\begin{bmatrix}\dot{x}\\ \dot{y}\\ \dot{\theta}\end{bmatrix}=\begin{bmatrix}\cos\theta & 0\\ \sin\theta & 0\\ 0 & 1\end{bmatrix}\begin{bmatrix}v\\ \omega\end{bmatrix} \tag{4}$$

The relationship between the rotational angular speeds w_1 and w_2 of the robot driving wheel and the position coordinates of the robot p point in the global coordinate system is expressed as:

$$\dot{q}=\begin{bmatrix}\dot{x}\\ \dot{y}\\ \dot{\theta}\end{bmatrix}=\begin{bmatrix}\frac{R}{2}\cos\theta & \frac{R}{2}\cos\theta\\ \frac{R}{2}\sin\theta & \frac{R}{2}\sin\theta\\ \frac{R}{2b} & -\frac{R}{2b}\end{bmatrix}\begin{bmatrix}w_1\\ w_2\end{bmatrix} \tag{5}$$

The kinematic model of the robot is developed and the relationship between the motion parameters of the driving wheel and the posture of the robot is analysed. This provides a theoretical basis for the flexible motion control experiment of the six-wheel rehabilitation robot.